Hydrodynamic and chemical effects of hydrogen dilution on soot evolution in turbulent nonpremixed bluff body ethylene flames

Sili Deng[a,*], Michael E. Mueller[a], Qing N. Chan[b], Nader H. Qamar[c], Bassam B. Dally[d], Zeyad T. Alwahabi[d], Graham J. Nathan[d]

[a] *Department of Mechanical and Aerospace Engineering, Princeton University, Princeton, USA*
[b] *School of Mechanical and Manufacturing Engineering, The University of New South Wales, Australia*
[c] *FCT-Combustion, Australia*
[d] *Centre for Energy Technology, The University of Adelaide, Australia*

Abstract

A turbulent nonpremixed bluff body ethylene/hydrogen (volume ratio 2 : 1) flame was studied and compared with the ethylene counterpart [Mueller *et al.* Combust. Flame, 160, 2013]. Similar to the ethylene buff body flame, a low-strain recirculation zone, a high-strain neck region, and a downstream jet-like region were observed. However, the maximum soot volume fraction in the recirculation zone and jet-like region of the hydrogen diluted case are significantly lower than the ethylene case. Steady flamelet calculation demonstrated the chemical effect on soot reduction, as hydrogen dilution surppresses soot formation due to the reduction of C/H ratio. A six times reduction was estimated, and it well predicted the reduction in the downstream jet-like region. However, soot reduction in the recirculation zone was underpredicted with this single effect, indicating additional hydrodynamic effect. Large Eddy Simulation was used to further investigate soot evolution in the recirculation zone and to elucidate the role of hydrogen dilution. Since the central jet Reynolds numbers in both cases are the same (approximately 30,900), the jet velocity of the hydrogen diluted case is higher, resulting in a shorter and leaner recirculation zone, which inhibits soot formation. Consequently, the reduction of the soot volume fraction for the hydrogen diluted ethylene flame is attributed to two major effects: hydrodynamic and chemical effects.

Keywords: Soot, Laser-induced incandescene, Large Eddie Simulation (LES), Bluff body flame, Turbulent nonpremixed flame

[*] Corresponding Author: silideng@princeton.edu

1. Introduction

Due to the importance of soot in practical transportation, propulsion, and power generation systems, the formation and growth of soot have been extensively studied. Most of these studies focus on laminar configurations, since flow conditions are better controlled and characterized, which enables detailed analysis of soot dynamics [1]. Soot evolution in turbulent reacting flows and the small-scale interactions among soot, turbulence, and chemistry has been aided by Direct Numerical Simulation (DNS). However, these studies are limited to two-dimensional, often with reduced chemistry and empirical soot model [2–6], due to the inherent complexity of chemical mechanisms, and hence, computational cost.

Recently, Attili *et al.* [7] performed the first three-dimensional DNS of turbulent nonpremixed jet flames employing a high-order statistical model of soot and detailed chemical mechanism, which includes the soot precursor naphthalene, and investigated Damköhler number effects on soot formation and growth [8]. Nevertheless, the Reynolds number is limited to $15,000$, and the jet flame configuration does not contain more complex fluid dynamics found in practical combustion systems as recirculation flow.

Therefore, detailed experimental data are needed to validate models for soot evolution in practical turbulent reacting flows. Mueller *et al.* [9] experimentally and computationally studied a turbulent nonpremixed bluff body ethylene flame. The Large Eddie Simulation (LES) model for sooting flames was validated for a piloted natural gas jet diffusion flame, the Delft III flame [10], and ethylene was chosen in the bluff body study to avoid large uncertainties in soot precursor chemistry in methane flames. Laser-induced incandescence (LII) was used to measure soot volume fraction.

In the present work, the hydrogen diluted ethylene sooting flame with the same bluff body configuration is investigated. During the thermal decomposition of hydrocarbon fuels, it has been shown that the dilution of hydrogen slows down the formation of soot [11]. Ever since then, extensive laminar studies have been conducted with simplified flow conditions to understand the overall suppression of soot formation in hydrogen diluted diffusion flames and attribute such suppression to both dilution and chemistry effects [12–16]. However, to maintain the same turbulence intensity as the ethylene bluff body flame [9], a stronger central jet is needed. Consequently, hydrodynamic effects should also be considered to understand soot-turbulence-chemistry interactions.

The objective of the this investigation is threefold: first, to understand the evolution of soot in the hydrogen diluted ethylene bluff body flame utilizing a combination of experiments and computations; second, to assess differences between hydrogen diluted and neat ethylene flames and further validate the LES model; and third, to differentiate the hydrodynamics and chemical effects by hydrogen addition.

2. Experimental methodology

The experimental setup used in the current study is similar to previous bluff body studies [17, 18], and was kept the same as the previous ethylene case [9]. In brief, the outer diameter of the bluff body (D_B) is 50 mm, and the diameter (D_J) of the central fuel jet is 3.6 mm, where ethylene/hydrogen mixture ($2:1$ by volume) is issued at 102.1 m/s. Compared with the 74.2 m/s ethylene jet velocity in the previous study [9], the increased jet velocity compensated the density decrease, and therefore ensured approximately the same Reynolds number of $30,900$. The bluff body burner was mounted in a contraction with an exit cross section of 150 by 150 mm^2, where air coflow is issued at 23 m/s.

The 1064 nm beam from an Nd:YAG laser was used for LII excitation. The laser sheet has a height of 80 mm through the measurement volume and has a thickness of 0.3 mm. The operating LII fluence was kept at 0.9 J/cm^2 to ensure the independence of the laser fluence variation [19, 20]. A Gaussian distribution of the spatial fluence with a 8% standard deviation was achieved. All images presented in this work have been clipped at the edges where the laser sheet was found to exhibit low fluence.

The LII signal was filtered at 430 ± 10 nm and detected by an intensified CCD camera. A short gate width of 40 ns was used to reduce the size-dependent sensitivity of the signal [21]. The LII signal has been calibrated by laser extinction measurement previously [9]. With this system, the in-plane resolution of the images is 0.26 mm/pixel in each direction, and the detection threshold is about 3 ppb.

The data presented in this work have been corrected for background interference and detector attenuation. According to the previous ethylene bluff body study, the estimated measurement uncertainty is about 25%.

3. Computational methodology

The modeling of soot-chemistry-turbulence interactions is aided by a statistical soot model, a Radiation

Flamelet/Progress Variable (RFPV) combustion model, and a presumed subfilter PDF for closure. Complete details of the integrated LES model for sooting turbulent nonpremixed flames can be found in Mueller and Pitsch [10] and the references therein.

In brief, soot particles and aggregates are described by their volume (V) and surface area (S), and transport equations are solved for the bivariate moment, $M_{x,y} = \sum_i V_i^x S_i^y N_i$, where x and y are the moment orders for volume and surface area, and summation over i implies summation over all particle sizes. Comprehensive physical and chemical processes governing the evolution of the moments are considered: particle nucleation from Polycyclic Aromatic Hydrocarbon (PAH) dimers [22–24], PAH condensation, particle coagulation [25], surface growth by C_2H_2-addition (HACA) mechanism [26], oxidation [27, 28], and oxidation-induced fragmentation [29]. Moment closure is achieved with the Hybrid Method of Moments (HMOM) [25]. In total, four quantities are used to describe the evolution of the soot population: the total soot number density ($M_{0,0}$), the total soot volume ($M_{1,0}$), the total soot surface area ($M_{0,1}$), and the number density of smaller particles (N_0).

The thermochemical states, such as temperature, species mass fractions (Y), and other derived quantities, are obtained from tabulated chemistry, described with the RFPV model of Ihme and Pitsch [30]. Solutions of the steady flamelets equations are parameterized by the mixture fraction (Z), a reaction progress variable ($C = Y_{CO_2} + Y_{CO} + Y_{H_2O} + Y_{H_2}$), and a heat loss parameter (H, which is zero when radiation source is zero), to account for heat losses due to radiation. Due to significant unsteady effects for PAH [6], the mass fractions for these species deviate from their steady values in the flamelet database. Therefore, an additional transport equation for a lumped PAH species is solved.

The closure for filtered quantities such as density, gas-phase source terms, and soot source terms are achieved with a presumed subfilter PDF model by Mueller and Pitsch [10, 31]. The joint subfilter of the mixture fraction, progress variable, heat loss parameter, and soot moments ($\widetilde{P}(Z, C, H, M_i)$) can be modeled by the product of the thermochemical subfilter PDF, $\widetilde{P}(Z, C, H)$, and the soot subfilter PDF, $\widetilde{P}(M_i)$, due to the time scale decoupling for the gas-phase and soot evolution [31]. The thermochemical PDF is modeled with a beta distribution for the mixture fraction [32]. Convolution of the flamelet database with the PDF is done *a priori* and tabulated as a function of the filtered mixture fraction, subfilter mixture fraction variance, filtered progress variable, and filtered heat loss parameter. The subfilter mixture fraction variance is obtained from the solution of a transport equation for the filtered squared of the mixture fraction with a linear relaxation model [33]. The soot subfilter PDF is modeled with a double delta distribution [31], which requires solving an additional transport equation for the filtered square of the number density.

In summary, the continuity, momentum equations, and transport equations for $\widetilde{Z}$, $\widetilde{Z^2}$, $\widetilde{C}$, $\widetilde{H}$, $\widetilde{Y_{\mathrm{PAH}}}$, $\overline{M_{0,0}}$, $\overline{M_{1,0}}$, $\overline{M_{0,1}}$, $\overline{N_0}$, and $\overline{M_{0,0}^2}$ are solved in the simulation. All of the subfilter stresses and scalar fluxes are closed with dynamic models [34] with Lagrangian averaging [35]. The soot unknown moments are closed with HMOM, and density, gas-phase, and soot source terms are closed with presumed subfilter PDF.

The simulation details are similar to the previous ethylene bluff body flame [9]. Flamelet solutions were computed using FlameMaster [36] with the chemical mechanism, including PAH, of Pitsch and coworkers [37, 38]. The soot and combustion models were implemented in NGA [39]. The continuity and momentum equations are discretized with a centered, second-order scheme, and the scalar equations are discretized with a bounded QUICK scheme [40]. The computational domain is discretized on a structured, nonuniform grid, with $384 \times 192 \times 64$ points in the axial, radial, and circumferential directions, respectively. To be consistent with the neat ethylene case, turbulence intensity in the central jet is increased by 10%, and turbulent boundary layer condition for the coflow is specified.

4. Results and discussion

4.1. Overall flame structure

The overall structure of the turbulent nonpremixed hydrogen diluted ethylene bluff body flame is demonstrated in Fig. 1. Similar to the ethylene counterpart, qualitatively, three distinct regions are identified: a sooting recirculation zone, a non-sooting, high strain neck region, and a jet-like downstream. Quantitatively, the clipped, time-averaged LII images of soot volume fraction were presented. Soot is formed close to the bluff body, where the residence time is long and turbulence intensity is low. No detectable soot is convected to nor formed in the high strain neck region. Further downstream in the jet-like region, where the scalar dissipation rate decreases as mixing proceeds, soot formation is activated.

Although share similar flow and soot formation patterns, the ethylene/hydrogen flame is significantly less sooting than the neat ethylene flame. As demonstrated

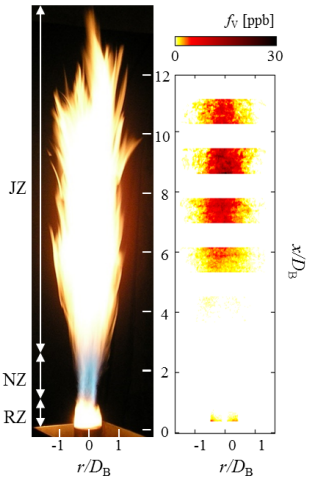

Figure 1: Left: photograph of the ethylene/hydrogen bluff body flame. Three distinct regions are indicated: RZ (recirculation zone), NZ (neck zone), and JZ (jet-like zone). Right: collage of the time-averaged LII images of the soot volume fraction distribution.

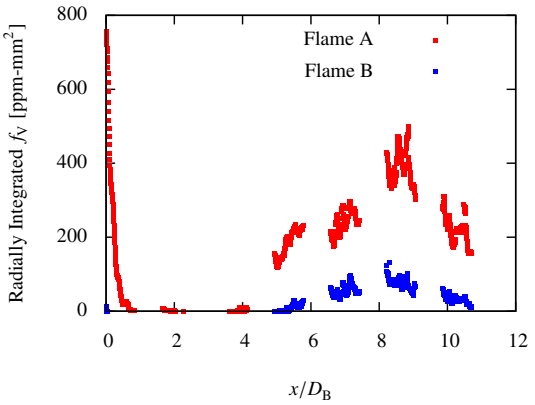

Figure 2: Total soot volume per unit height obtained from the radial integration of the time-averaged soot volume fraction at each height for the ethylene (Flame A) and ethylene/hydrogen (Flame B) bluff body flames. For clarity, only every second measurement point is shown.

in Fig. 2, the axial profiles of the radially integrated soot volume fraction (ppm-mm^2) are compared for the two flames. Both profiles are bimodal, corresponding to the recirculation zone and jet-like region, respectively. Since the Reynolds number was kept nearly the same in both cases, the flame lengths and soot double-peak locations are almost identical. However, both peaks in the hydrogen diluted flame is reduced. Furthermore, the reduction in the integrated soot volume fraction is more pronounced in the recirculation zone, compared to the downstream jet-like region. Specifically, according to both Figs. 1 and 2, the soot reduction in the recirculation zone is more than an order of magnitude, while in the jet-like zone, the reduction is about five times. The difference in the soot reduction rate with hydrogen dilution indicates different soot reduction mechanisms and different roles that hydrogen dilution plays in these two regions.

4.2. Effects of hydrogen dilution

Two effects of hydrogen dilution are potentially relevant: chemical and hydrodynamic effects. Chemically, due to the reduced C/H ratio, PAH formation might be inhibited in the hydrogen diluted flame, and therefore, soot formation is inhibited. Hydrodynamically, since the fuel jet velocity is increased to match the Reynolds number, the fuel to air coflow momentum flux ratio is also increased. As Dally *et al.* [41] demonstrated, the increase in the fuel jet momentum flux decreases the strength of the mixture in the outer vortex in the recirculation zone and shifts the stoichiometric mixture fraction contour closer to central jet. Such shift might result in a relatively leaner recirculation zone, and therefore inhibit soot formation.

To justify and differentiate these effects, steady flamelets at a moderate scalar dissipation rate (χ = 10/s) was calculated and presented in Fig. 3. PAH forms at rich mixture fractions (the stoichiometric mixture fraction for both cases is about 0.06) and peaks at Z = 0.23. Y_{PAH} decreases at even richer mixture fractions due to the temperature drop. Comparing the peak values of Y_{PAH}, hydrogen dilution results in a 2.5 times decrease. Bisetti *et al.* [6] and Attili *et al.* [7, 8] showed through DNS studies that PAH based growth (PAH dimer nucleation and condensation) accounts for most of the soot mass while growth due to acetylene via the HACA mechanism is less important for the jet-like configuration. In addition, in the soot model adopted in this LES study, the PAH based growth rate scales with square of PAH concentration [10]. Consequently, roughly a 6 times soot volume fraction decrease is expected due to the chemical effect. This agrees with trend in the reduction rate in the jet-like region, and chemical effect is dominant in this region.

Conversely, noting that the chemical effect predicted by the steady flamelet solution cannot explain the additional soot reduction in the recirculation zone, soot evolution in this region is further analyzed. The time-averaged soot volume fraction in the recirculation zone from the LES is compared between the neat and hydrogen diluted ethylene flames in Fig. 4. For both cases, soot is confined to fuel-rich regions. In accordance with the trend of the radially integrated soot volume fraction in Fig. 2, significant soot reduction is observed in the

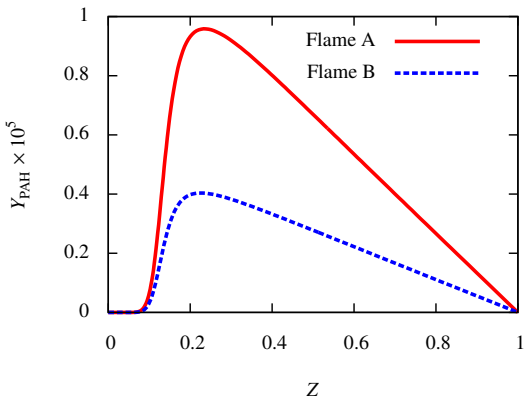

Figure 3: PAH mass fraction profile from the steady flamelet calculation at $\chi = 10$/s for the ethylene (Flame A) and ethylene/hydrogen (Flame B) bluff body flames.

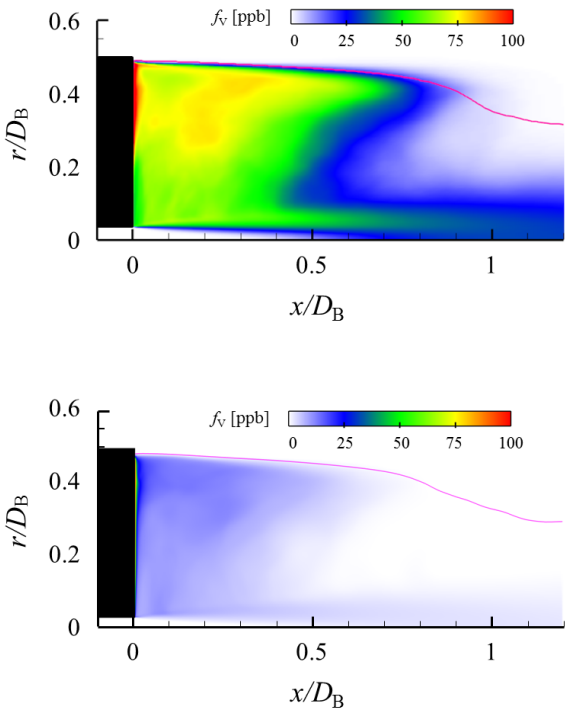

Figure 4: Time-averaged soot volume fraction [ppb] in the recirculation zone of ethylene (top) and ethylene/hydrogen (bottom) flames. The magenta line correspond to the stoichiometric mixture fraction contour.

hydrogen diluted case. Specifically, radial profiles of the time-averaged soot volume fraction are compared for both cases at two axial locations in the recirculation zone, shown in Fig. 5.

Overall agreement between the experimental measurement and LES results is good. Qualitatively, a bimodal radial distribution is found. Mueller *et al* [9] found in the ethylene bluff body flame that the inner and outer peak corresponds to the PAH-based growth and acetylene-based surface growth pathway, respectively. Quantitatively, the soot volume fraction of the ethylene case is slightly underpredicted, but within experimental uncertainty [9]. However, for the hydrogen diluted case, soot volume fraction is overpredicted. In the experiments, the most upstream laser measurement location is slightly less than $0.5D_B$ due to the laser scattering from the bluff body surface. Moreover, due to the increased fuel jet velocity, the length of the recirculation zone is shorter. As a consequence, the measurement locations in the relatively high soot loading region within the recirculation zone are limited. Noting that in Fig. 2, the slope of the integrated soot volume fraction profile in the recirculation zone is very steep. Therefore, the experimental uncertainty might increase in this region for the hydrogen diluted flame.

To elucidate the hydrodynamic effects on soot reduction, the characteristic rates of the soot formation and oxidation processes from a slighted strained ($\chi = 0.01$/s) steady flamelet solution as well as the mixture fraction radial profiles from LES are shown in Fig. 6. The characteristic rates of the PAH-based growth, acetylene-based growth, and oxidation are shown on the left sub-figure. Negligible difference is found between the neat and hydrogen diluted flames, in terms of both the magnitudes of these scales and the distributions of these profiles. In the recirculation zone, close to the central jet, where mixture fraction is above 0.2, the PAH-based growth is dominant. The acetylene-based pathway takes over at $Z = 0.15$, as mixture fraction is reduced due to the entrainment of the coflow air. In between $Z = 0.15$ and 0.2, the mixture fraction is too low to support maximum PAH formation yet too high for appreciable acetylene-based surface growth. Oxidation is negligible near the bluff body, until the stoichiometry mixture fraction contour shifts towards the central jet prior to the neck region.

Although the characteristic rates of the soot evolution processes merely change due to hydrogen dilution, the mixture fraction profile near the bluff body surface is affected substantially. As shown in Fig. 6, in between the central jet and coflow air, mixture fraction drops by 20%, indicating that less fuel and more coflow is filled near the bluff body surface due to the hydrodynamic effect. The mixture fraction profile of the hydrogen diluted flame mainly falls into the region where

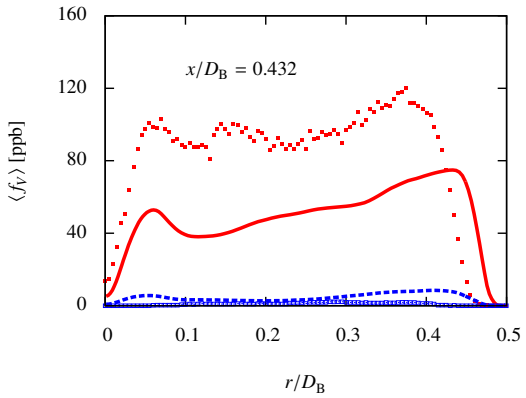

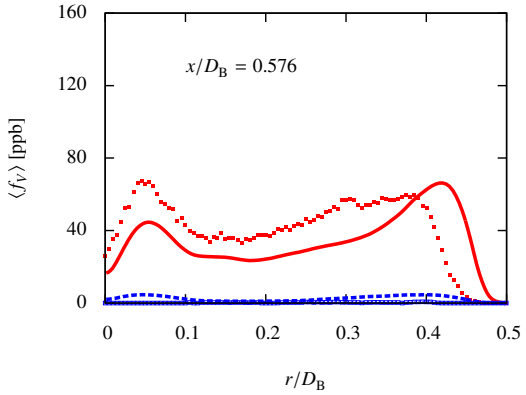

Figure 5: Radial profiles of the time-averaged soot volume fraction. Lines are the LES, and symbols are the measurements. The ethylene flame (red solid line and red closed symbol) is reproduced from [9], and the ethylene/hydrogen flame is from this work (blue dashed line and blue open symbol).

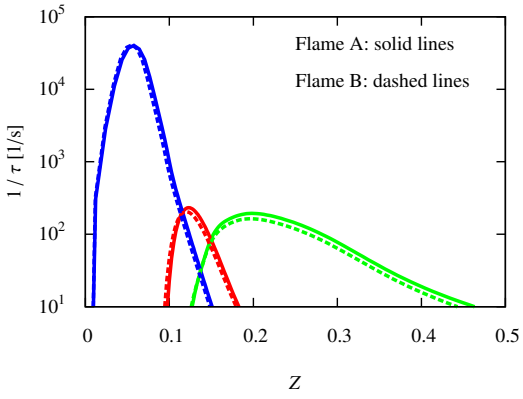

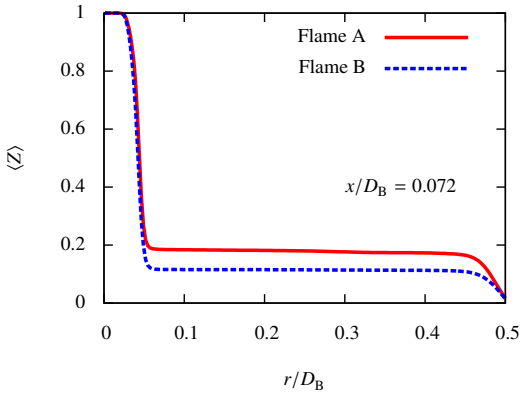

Figure 6: Left: characteristic inverse time scales of the soot processes from the steady flamelet calculations at $\chi = 0.01$/s. Solid lines are for the ethylene flame (Flame A), and dashed lines are for the ethylene/hydrogen flame (Flame B). Oxidation process is in blue, surface growth is in red, and nucleation and condensation combined is in green. Right: radial profile of the time-averaged mixture fraction.

both PAH-based and acetylene-based growth rates are relatively small, according to the characteristic inverse time scale plot in Fig. 6. Therefore, soot formation in the recirculation zone is further inhibited by this hydrodynamic effect, in addition to the chemical effect.

This conclusion is further elucidated in the PAH-based growth source term analysis, shown in Fig. 7. As discussed previously, a 6 times PAH-based growth source term reduction is expected due to the chemical effect on PAH concentration from the steady flamelet analysis. Therefore, the legend values in the hydrogen diluted case are reduced by 6 times, such that a direct color comparison better demonstrates any additional hydrodynamic effect on the source term. Noting from Fig. 6, the increase jet velocity has minimal effect on the mixture fraction near the bluff body surface and central jet, the local PAH-based growth source term should mainly be affected by the chemical effect on PAH concentration reduction. Indeed, the color pattern near the central jet exit matches between two flames. Conversely, the source term decrease is even more, with the chemical effect already being accounted, between $r/D_B = 0.1$ and 0.4, which agrees with the decrease in mixture fraction in Fig. 6. This again demonstrates the additional hydrodynamic effect on soot reduction due to increased jet velocity.

5. Conclusions

A sooting turbulent bluff body stabilized ethylene/hydrogen flame was studied both experimentally and computationally and compared with a previously analyzed ethylene counterpart [9]. Laser-induced incandescence (LII) was utilized to measure the soot volume fraction in the flame. A integrated Large Eddie Simulation (LES) model was adopted to elucidate the inter-

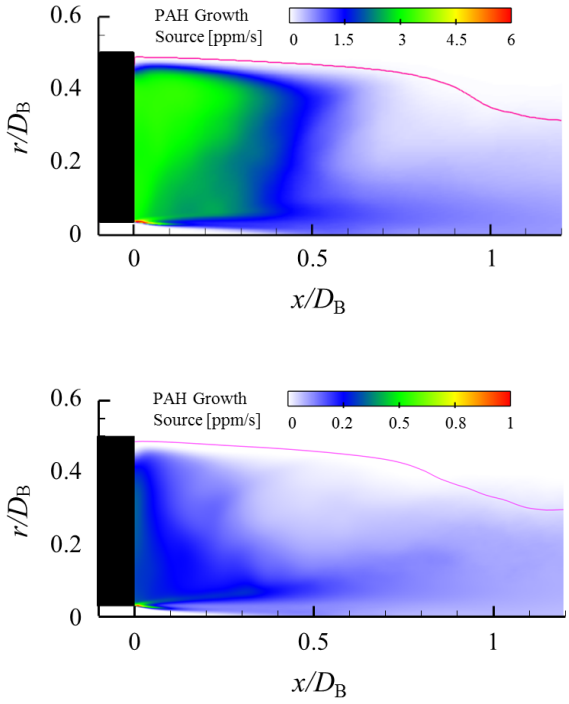

Figure 7: Time-averaged soot volume fraction source term [ppm/s], including both PAH dimer nucleation and condensation, in the recirculation zone of ethylene (top) and ethylene/hydrogen (bottom) flames. Note that the color legend of the ethylene/hydrogen flame is scaled down by six times. The magenta line correspond to the stoichiometric mixture fraction contour.

actions between soot, turbulence, and chemistry. The statistical soot model was based on the Hybrid Method of Moments (HMOM), considering detailed nucleation, condensation, particle collision, surface growth, oxidation, and fragmentation processes that influence soot evolution. The combustion model for the gas-phase was based on the Radiation Flamelet/Progress Variable (RFPV) model with modifications to account for the Polycyclic Aromatic Hydrocarbon (PAH) removal from the gas-phase. A presumed PDF was utilized to model unresolved subfilter scale interactions.

Similar to the ethylene bluff body flame, three distinct flow regions were observed experimentally: a sooting recirculation zone, a non-sooting, high strained neck region, and a sooting jet-like downstream. Although the hydrogen diluted bluff body flame is significantly less sooting than the ethylene counterpart overall, soot reduction in the recirculation zone near the bluff body is more pronounced compared to the downstream jet-like region. Both chemical and hydrodynamic effects were identified and elucidated in this work.

The chemical effect was benchmarked from a slighted strained steady flamelet calculation. Due to the hydrogen addition, PAH mass fraction was found to decrease by a factor of 2.5, indicating a 6 times decrease in the PAH-based growth rate that includes both PAH dimer nucleation and condensation. This agrees with the soot reduction rate in the downstream jet-like region, where PAH-based growth is dominant. Therefore, the chemical effect is dominant in this region.

Conversely, both the experimental measurement and soot production source term analysis in LES demonstrated additional soot reduction in the recirculation zone, which could not be explained based on the chemical effect. In the experiment, to remain the same Reynolds number in the hydrogen diluted flame as the ethylene flame, the central jet velocity was increased. This increase in the fuel to air coflow momentum flux ratio allows relatively less fuel and more air in the recirculation zone near the bluff body surface, compared to the ethylene flame. As a consequence, soot formation is inhibited due to leaner mixture fraction in the recirculation zone. This hydrodynamic effect together with the chemical effect accounts for the soot reduction in the recirculation zone.

Acknowledgments

Thanks M for the helpful discussion and figures for the ethylene flame.

References

[1] H. Wang, Proc. Combust. Inst. 33 (2011) 41–67.
[2] H. Pitsch, E. Riesmeier, N. Peter, Combust. Sci. Technol. 158 (2000) 389–406.
[3] C. S. Yoo, H. G. Im, Proc. Combust. Inst. 31 (2007) 701–708.
[4] D. O. Lignell, J. H. Chen, P. J. Smith, T. Lu, C. K. Law, Combust. Flame 151 (2007) 2–28.
[5] D. O. Lignell, J. H. Chen, P. J. Smith, Combust. Flame 155 (2008) 316–333.
[6] F. Bisetti, G. Blanquart, M. E. Mueller, H. Pitsch, Combust. Flame 159 (2012) 317–335.
[7] A. Attili, F. Bisetti, M. E. Mueller, H. Pitsch, Combust. Flame 161 (2014) 1849–1865.
[8] A. Attili, F. Bisetti, M. E. Mueller, H. Pitsch, Proc. Combust. Inst. 35 (2015) 1215–1223.
[9] M. E. Mueller, Q. N. Chan, N. H. Qamar, B. Dally, H. Pitsch, Combust. Flame 160 (2013) 1298–1309.
[10] M. E. Mueller, H. Pitsch, Combust. Flame 159 (2012) 2166–2180.
[11] P. A. Tesner, Proc. Combust. Inst. 7 (1958) 546–553.
[12] P. Dearden, R. Long, J. Appl. Chem. 18 (1968) 243–251.
[13] D. X. Du, R. L. Axelbaum, C. K. Law, Comb. Flame 102 (1995) 11–20.
[14] O. L. Gülder, D. R. Snelling, R. A. Sawchuk, Proc. Combust. Inst. 26 (1996) 2351–2358.

[15] H. Guo, F. Liu, G. J. Smallwood, O. L. Gülder, Combust. Flame 145 (2006) 324–338.
[16] H. Zhao, R. Stone, B. Williams, Energy Fuels 28 (2014) 2144–2151.
[17] B. B. Dally, A. R. Masri, R. S. Barlow, G. J. Fiechtner, D. F. Fletcher, Proc. Combust. Inst. 26 (1996) 2191–2197.
[18] B. B. Dally, D. F. Fletcher, A. R. Masri, Combust. Theor. Model. 2 (1998) 193–219.
[19] N. H. Qamar, Z. T. Alwahabi, Q. N. Chan, G. J. Nathan, D. Roekaerts, K. D. King, Combust. Flame 156 (2009) 1339–1347.
[20] C. Schulz, B. F. Kock, M. Hofmann, H. Michelsen, S. Will, B. Bougie, R. Suntz, G. Smallwood, Appl. Phys. B 83 (2006) 333–354.
[21] H. Bladh, P. E. Johnsson, J. Bengtsson, Appl. Phys. B 90 (2008) 109–125.
[22] C. A. Schuetz, M. Frenklach, Proc. Combust. Inst. 29 (2002) 2307–2314.
[23] D. Wong, C. A. Schuetz, M. Frenklach, in: H. Bockhorn, A. D'Anna, A. Sarofim, H. Wang (Eds.), Combustion Generated fine Carbonaceous Particles, KIT Scientific Publishing, 2009, pp. 247–257.
[24] G. Blanquart, H. Pitsch, in: H. Bockhorn, A. D'Anna, A. Sarofim, H. Wang (Eds.), Combustion Generated fine Carbonaceous Particles, KIT Scientific Publishing, 2009, pp. 439–466.
[25] M. E. Mueller, G. Blanquart, H. Pitsch, Combust. Flame 156 (2009) 1143–1155.
[26] M. Frenklach, H. Wang, Proc. Combust. Inst. 23 (1991) 1559–1566.
[27] A. Kazakov, H. Wang, M. Frenklach, Combust. Flame 100 (1995) 111–120.
[28] K. G. Neoh, J. B. Howard, A. F. Sarofim, in: Particulate Carbon Formation during Combustion, Plenum Press, 1981, pp. 162–282.
[29] M. E. Mueller, G. Blanquart, H. Pitsch, Proc. Combust. Inst. 33 (2011) 667–674.
[30] M. Ihme, H. Pitsch, Phys. Fluids 20 (2008) 055110.
[31] M. E. Mueller, H. Pitsh, Phys. Fluids 23 (2011) 115104.
[32] A. W. Cook, J. J. Riley, Phys. Fluids 6 (1994) 2868–2870.
[33] M. Ihme, H. Pitsch, Combust. Flame 155 (2008) 90–107.
[34] M. Germano, U. Piomelli, P. Moin, W. H. Cabot, Phys. Fluids A 3 (1991) 1760–1765.
[35] C. Meneveau, T. S. Lund, W. H. Cabot, J. Fluid Mech. 319 (1996) 353–385.
[36] H. Pitsch, FlameMaster, a C++ computer program for 0D combustion and 1D laminar flame calculations.
[37] G. Blanquart, P. Pepiot, H. Pitsch, Combust. Flame 156 (2009) 588–607.
[38] K. Narayanaswamy, G. Blanquart, H. Pitsch, Combust. Flame 157 (2010) 1879–1898.
[39] O. Desjardins, G. Blanquart, G. Balarac, H. Pitsch, J. Comput. Phys. 227 (2008) 7125–7159.
[40] M. Herrmann, G. Blanquart, V. Raman, AIAA J. 44 (2006) 2879–2886.
[41] B. B. Dally, A. R. Masri, R. S. Barlow, G. J. Fiechtner, Combust. Flame 114 (1998) 119–148.